J. Synchrotron Rad. (1997). **4**, 102–109

High-Energy Magnetic Compton Scattering from Iron

J. E. McCarthy,[a,b] M. J. Cooper,[b] P. K. Lawson,[b] D. N. Timms,[c] S. O. Manninen,[d] K. Hämäläinen[d] and P. Suortti[a]

[a]European Synchrotron Radiation Facility, BP 220, F-38043 Grenoble CEDEX, France, [b]Department of Physics, University of Warwick, Coventry CV4 7AL, UK, [c]Division of Physics, University of Portsmouth, Portsmouth PO1 2DZ, UK, and [d]Department of Physics, PO Box 9, FIN-00014 University of Helsinki, Finland. E-mail: csmc@spec.warwick.ac.uk

(*Received 8 June 1996; accepted 2 December 1996*)

The magnetic Compton profile of Fe [111] was measured using circularly polarized synchrotron radiation at incident energies of 84.4, 167.2 and 256.0 keV on the high-energy beamline at the European Synchrotron Radiation Facility. It was found that the momentum resolution of these experiments, which use semiconductor detectors, improves by almost a factor of two over what was previously possible by this technique at photon energies of $\sim(1/10)mc^2$. It was also observed that all three spectra reduced to the magnetic Compton profile, describing the spin-dependent ground-state momentum density, and that within the experimental error the integrated intensity of the magnetic effect scaled as predicted by the cross section derived in the limit of energies much less than the rest energy of the electron. The magnetic Compton profile of Fe [111], measured using 167.2 keV incident energy and with momentum resolution of 0.42 a.u., was compared with the prediction from a full-potential linearized augmented-plane-wave model profile. The fine structure predicted by theory was confirmed by the experimental profile at this improved resolution.

Keywords: Compton scattering; ferromagnetism; iron; magnetic Compton profile; spin density.

1. Introduction

Within the impulse approximation the spectrum of inelastically scattered unpolarized radiation can be interpreted in terms of the ground-state electron momentum distribution of all the electrons in the target according to the equations given in §2 below. In magnetic Compton scattering, the use of circularly polarized photons allows the momentum density of those electrons with unpaired spin to be isolated in ferromagnetic or ferrimagnetic materials; since Compton scattering is an incoherent process, no magnetic effect is observed in antiferromagnets. Although these experiments are now performed with synchrotron radiation, the method was first demonstrated by Sakai & Ôno (1976) (see also Sakai, Terashima & Sekizawa, 1984) who used a cooled beta-emitter radioisotope as the source. Their pioneering work was paralleled in the diffraction case by De Bergevin & Brunel (1972, 1981) who used unpolarized X-ray tube sources.

The formula for the cross section for elastic and inelastic magnetic X-ray scattering was first developed by Platzman & Tzoar (1970). Their work and that which followed was developed in the approximation that $E_i << mc^2$, where E_i is the energy of the incident photon and mc^2 is the rest energy of the electron (see, for example, Grotch, Kazes, Bhatt & Owen, 1983; Blume, 1985; Lovesey, 1993; Sakai, 1996). The cross section for diffraction has also been specifically calculated for different polarization components (see Blume & Gibbs, 1988; Lovesey, 1987, 1993). The well established formulae for diffraction include contributions from both the spin, **S**, and orbital, **L**, magnetization of the scatterer, which are separable because of their different angular dependencies. In diffraction studies there is usually no incentive to go beyond the conventional X-ray energy range (5–25 keV) for three reasons. First, the magnetic effect scales with the momentum transfer, not the energy transfer, and that is fixed for a particular Bragg reflection. Second, the Bragg angles become inconveniently small at high energies, and third, resonances associated with the *K*, *L* and *M* edges of most targets are already accessible at the lower energies. Two exceptions are the white-beam method for ferromagnets (see, for example, Zukowski *et al.*, 1992), where there is evidence that there is a magnetic effect associated with the high-order (*i.e.* high momentum transfer) reflections in Ni, and methods which take advantage of the 'special geometry' afforded by small scattering angles to separate **S** and **L** contributions to the magnetic moment (Bruckel, Lippert, Kohler, Schneider & Prandl, 1995; Bruckel, Bouchard *et al.*, 1995). The optimal energy for these diffraction studies is a compromise between decreasing photoelectric absorption, which permits a larger effective sample volume to be used at higher photon energies, and the decrease in monochromator and sample crystal reflectivity in addition to the usual decrease in source

flux with photon energy. Whilst further development of these diffraction techniques will occur, it is unlikely that photon energies of much more than $(1/4)mc^2$ will be used.

In Compton-scattering studies there are fewer reasons to keep to low photon energies. The process is incoherent and therefore the scattering angle and the photon energy are independent variables. Thus, the magnetic cross section, which, at low energies at least, is approximately proportional to the momentum transfer, can be maximized by choosing the largest practicable scattering angle and the highest photon energy for which sufficient flux is available. The magnetic scattering cross section for inelastic (Compton) scattering from a free stationary electron was first calculated for all photon polarizations by Lipps & Tolhoek (1954). In this case, scattering must arise solely from spin magnetization: there is no possibility of a contribution from orbital magnetization for a free electron. The differential scattering cross section for a moving, relativistic, polarized free electron was calculated by Bhatt, Grotch, Kazes & Owen (1983) and some corrections for bound polarized electrons have recently been considered by Bell, Felsteiner & Pitaevskii (1996) following the method developed by Ribberfors (1975) for unpolarized bound electrons.

Initial experiments were performed on ferromagnets such as Fe and Ni which not only have relatively large magnetic moments per formula unit but also have their orbital moments quenched; not surprisingly, the results were interpreted solely in terms of spin magnetization (Mills, 1987; Cooper *et al.*, 1986; Timms *et al.*, 1990; Sakai *et al.*, 1991). More recently, studies of ferromagnetic rare-earth compounds such as $HoFe_2$, which do have large orbital moments, have been carried out in a series of experiments begun at the storage ring source, Daresbury, UK, but largely performed at the accumulation ring, KEK, Japan. These experiments sought to establish (*a*) that the magnetic Compton cross section is only sensitive to the spin moment **S** in ferromagnets (Cooper *et al.*, 1992; Timms *et al.*, 1993), (*b*) that individual site moments can be isolated (Zukowski *et al.*, 1993; Cooper *et al.*, 1993), and (*c*) to measure their temperature variation (Lawson *et al.*, 1995). The unique spin sensitivity of the method, which leads to cross sections similar to that predicted for free electrons, is essentially a consequence of the impulse approximation under which these experiments are performed; it has been discussed by several authors (Lovesey, 1993; Sakai, 1994; Carra, Fabrizio, Santoro & Thole, 1996) and is now well established. Although the term 'spin-dependent Compton profile' would be an appropriate description of what is actually measured, the name 'magnetic Compton profile' is widely used. The combination of these spin-density data with bulk magnetization results even allows some estimate of orbital moments to be made. Such studies complement magnetic neutron diffraction methods for materials with a net moment. The reader is referred to Sakai (1996) for the most recent comprehensive review of magnetic Compton scattering, and Cooper (1985) for background to Compton-scattering studies of electron momentum distributions.

There are at least two reasons for increasing the energy at which magnetic Compton-scattering measurements are performed. The first is to study the magnetic scattering cross section and discover whether it deviates from the prediction of theory developed for low energies. In this preliminary study, energies up to the order of $(1/2)mc^2$ were employed, the limit being set by the flux from the asymmetric wiggler which has a critical energy of 43 keV. Following the commissioning of the superconducting wavelength shifter at the ESRF, energies of $\sim$500 keV should be readily available and a test of the scattering theory will be possible. The second objective of this study was to determine an optimum energy for magnetic Compton-scattering experiments. At a practical level the strength of the magnetic scattering relative to the charge scattering increases with photon energy. This is important because the magnetic contribution to Compton scattering is very small compared with the charge contribution, magnetic effects being typically of the order of 1% of the charge effects for pure Fe at 60 keV, but less than 0.1% for compounds such as $CeFe_2$ and UFe_2 (Cooper *et al.*, 1996*a*,*b*) which have a much smaller ratio of unpaired to spin-paired electrons. These gains have to be weighed against the inevitable decline in flux delivered by the insertion device and beamline monochromator when the energy is raised.

As well as increasing the size of the magnetic effect, a higher incident energy also leads to an improvement in resolution when semiconductor detectors are used. Essentially, the width of the Compton profile scales linearly with the photon energy whereas the resolution function broadens with its square root. The resolution of magnetic Compton experiments is dominated by the contribution from these detectors, which have well known energy resolution characteristics (Sakai, 1992), and increased further by the need to have a broad geometrical acceptance and hence a range of Compton energy shifts for the scattered beam in order to maximize count rates. It is typically 0.6–0.8 a.u., which is poor since it is not much less than a typical Fermi momentum (1 atomic unit of momentum = 1.99×10^{-24} kg m s^{-1}; note that in atomic units h = 1 and c = 137). Prior to this work, only one magnetic Compton experiment had been performed at significantly higher resolution (0.12 a.u.) by Sakurai *et al.* (1994) who painstakingly used a dispersive crystal spectrometer to measure the magnetic Compton profile of Fe [110]. Unfortunately, the method still appears to be too slow for general exploitation at third-generation machines. We show below that, by choosing a higher incident energy, gains by a factor of two in experimental resolution can be achieved routinely with germanium detectors, rendering the interpretation more quantitative.

The sample used for these experiments was a single crystal of iron cut so that the (111) directional profile could be measured. It was chosen for a number of reasons: firstly, there is a full-potential linearized augmented-plane-wave (FLAPW) calculation by Kubo & Asano (1990) of directional magnetic Compton profiles which shows particular structure for this orientation which could not be

revealed in the earlier low-resolution studies; secondly, it has a large magnetic spin moment leading to a relatively large magnetic effect of the order of 1–2%; and thirdly, Fe is a soft ferromagnet and therefore is very easily magnetized.

In this paper, the basic cross section for magnetic Compton scattering is presented, the energy dependence of the ratio of magnetic to charge scattering is detailed, and the consequences of increasing the incident photon energy are discussed. Experimental measurements made on Fe [111] with three different incident energies are then analyzed and compared with the FLAPW theoretical calculation. Finally, the implications for future work are discussed.

2. The spin-dependent Compton cross section

The cross section for spin-dependent Compton scattering from a moving electron was first written down by Platzman & Tzoar (1970) (see also their review in 1985). They showed that the cross section could be written in the form

$$d^2\sigma/d\Omega dE = (e^2/mc^2)^2 S(\mathbf{K},E), \quad (1)$$

where $S(\mathbf{K},E)$ can be written

$$S(\mathbf{K},E) = \sum_{f,i} \left| \left\langle f \left| \sum_j M_j \exp(i\mathbf{K}.\mathbf{r}_j) \right| i \right\rangle \right|^2 \delta(E_s - E_i - E), \quad (2)$$

where E is the energy transfer $E_i - E_s$, E_i being the incident photon energy and E_s the scattered photon energy; the delta function expresses conservation of energy in what is assumed to be an impulsive binary encounter between the photon and electron.

The matrix elements, $\mathbf{M}_j$, for an electron with momentum $\mathbf{p}_j$ and spin $\mathbf{s}_j$ are of the form

$$A + \mathbf{C}.\mathbf{p}_j/(mc) + i\mathbf{B}.\mathbf{s}_j,$$

where A, $\mathbf{B}$ and $\mathbf{C}$ are functions of the polarization vectors of the incident and scattered photons. Here, it is only necessary to note that $|\mathbf{B}|$ is of the order of E_i/mc^2 and is imaginary if circular polarization is used, thus generating a real contribution to the cross section. Platzman & Tzoar (1970), and subsequent authors who treat the case of Compton scattering from a spin-polarized moving bound electron (Grotch *et al.*, 1983; Bhatt *et al.*, 1983; Lovesey, 1993; Sakai, 1996), restrict their attention to the term of order E_i/mc^2 which arises from the interference between the first and third terms in the matrix element [equation (3)]. This will also be true in the experiments reported here, but with the availability of devices such as the ESRF's superconducting wavelength shifter, which has a characteristic energy of 100 keV and is therefore capable of producing useful flux at energies above mc^2, it will become necessary to consider the spin-dependent Compton cross section at these energies.

As noted by Sakai (1996), the interference term calculated by all the above authors has the same form as the Klein–Nishina cross section quoted by Lipps & Tolhoek (1954) for the scattering from a free stationary electron. The latter is

$$\begin{aligned} d\sigma/d\Omega = {} & (1/4)(e^2/mc^2)^2(k_s/k_i)^2\{1 + \cos^2\theta \\ & + [(k_i - k_s)/mc](1 - \cos\theta) + P_l \sin^2\theta \\ & - P_c(1 - \cos\theta)\,\boldsymbol{\sigma}.(\mathbf{k}_i \cos\theta + \mathbf{k}_s)/mc\}, \end{aligned} \quad (3)$$

where $\mathbf{k}_i$ and $\mathbf{k}_s$ are the incident- and scattered-beam wavevectors, respectively, θ is the angle of scattering (the scattering geometry is defined in Fig. 1), and $\boldsymbol{\sigma}$ is a unit vector in the direction of the magnetization. The quantum-mechanical calculations for bound spin-polarized electrons lead to an expression for the double-differential cross section which is

$$\begin{aligned} d^2\sigma/d\Omega dE_s = {} & (e^2/mc^2)^2(m/2\hbar K)(E_s/E_i) \\ & \times \{f_1 J(p_z) + (\cos\theta - 1)P_c \\ & \times \boldsymbol{\sigma}.[(\mathbf{k}_i \cos\theta + \mathbf{k}_s)/mc]J_{\rm mag}(p_z)\}, \end{aligned} \quad (4)$$

where

$$f_1 = 1 + \cos^2\theta + [(E_i - E_s)/mc^2](1 - \cos\theta) + P_l \sin^2\theta,$$

and P_c and P_l are the degree of circular and linear polarization, respectively, of the incident beam.

The factor $(m/2\hbar K)$, which converts the momentum-dependent cross section to an energy-dependent one in equation (4), is in fact a low-energy approximation. At high energies, a more accurate expression is $m/2\hbar K[1 + E_i/mc^2(1 - \cos\theta)]$.

The Compton profile, $J(p_z)$, is defined as the projection of the total ground-state momentum density along the scattering vector (chosen as the z direction):

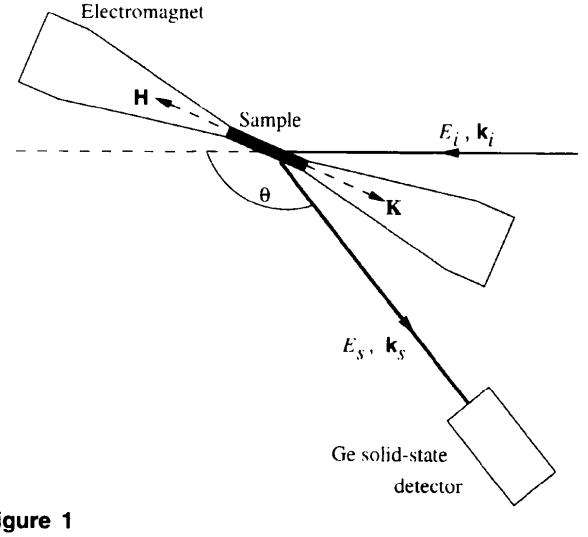

Figure 1
The scattering geometry for magnetic Compton experiments. The [110] single crystal is clipped between the pole pieces of an electromagnet and the [111] direction brought into parallel with the scattering vector by rotating the crystal. The scattering vector $\mathbf{K} = \mathbf{k}_i - \mathbf{k}_s$ is parallel to the direction of the magnetic field $\mathbf{H}$. The scattering angle is θ and the incident and scattered energy (momentum) are given by E_i, $\mathbf{k}_i$ and E_s, $\mathbf{k}_s$, respectively.

Table 1
Experimental parameters for each incident energy, including incident flux, data-collection time, the scattered beam count rates and the size of the magnetic effect, R, as defined in the text.

The errors quoted for the predicted values of R are estimated from consideration of the uncertainties in P_c.

E_i (keV)	Flux at sample position (photons s^{-1})	Collection time (h)	Counts under Compton peak	Peak count rate into detector (counts s^{-1})	Polarization P_c (%)	Magnetic effect Observed (%)	Magnetic effect Predicted (%)
84.4	4×10^{10}	8	1×10^{8}	10 500	44	0.81 (1)	0.83 (5)
167.2	5×10^{9}	12.5	5×10^{7}	2300	51	1.45 (1)	1.61 (10)
256.0	5×10^{8}	13	4×10^{6}	23	51	1.99 (4)	2.10 (13)

$$J(p_z) = \iint [n\uparrow(\mathbf{p}) + n\downarrow(\mathbf{p})]\, \mathrm{d}p_x \mathrm{d}p_y$$

and

$$\int_{-\infty}^{+\infty} J(p_z)\, \mathrm{d}p_z = Z, \tag{5}$$

where p_x, p_y and p_z are the momentum components in the x, y and z directions, and $n\uparrow(\mathbf{p})$ and $n\downarrow(\mathbf{p})$ are the momentum densities of majority-spin and minority-spin electrons, respectively; Z is the number of electrons per formula unit. The electron momentum, p_z, is related to the photon energies and the scattering angle by the equation

$$\frac{p_z}{mc} = \frac{E_s - E_i + [E_i E_s(1 - \cos\theta)/mc^2]}{(E_i^2 + E_s^2 - 2E_i E_s \cos\theta)^{1/2}}. \tag{6}$$

The magnetic Compton profile, $J_{\mathrm{mag}}(p_z)$, is the projection of the ground-state spin-dependent momentum distribution along the scattering vector (*i.e.* the contribution from the unpaired electrons only), hence

$$J_{\mathrm{mag}}(p_z) = \iint [n\uparrow(\mathbf{p}) - n\downarrow(\mathbf{p})]\, \mathrm{d}p_x \mathrm{d}p_y,$$

and

$$\int_{-\infty}^{+\infty} J_{\mathrm{mag}}(p_z)\, \mathrm{d}p_z = F_s, \tag{7}$$

where F_s is the spin moment (*i.e.* number of unpaired electrons) per formula unit.

In the experiments reported below, the magnetic signal is isolated by reversing the direction of the spins, because the charge scattering is unaffected by the spin direction. It is possible to predict the size of the magnetic effect at the different energies employed for the measurements from equation (4), always assuming that the low-energy approximations remain valid up to energies of the order of $(1/2)mc^2$. For these experiments, an increase by more than a factor of two is predicted and this in itself quarters the time needed to obtain a given statistical accuracy in the difference signal.

3. Experimental procedure

3.1. *The beamline and spectrometer*

These measurements were carried out on the high energy beamline at the ESRF, using a seven-period asymmetric multipole wiggler with a peak brightness of 2.5×10^{14} photons s^{-1} mrad^{-2} (0.1% bandwidth)$^{-1}$ and a critical energy of 43 keV (*ESRF Beamline Handbook*, 1994). Circularly polarized synchrotron radiation with $P_c \simeq 0.5$ (the calculated values are quoted in Table 1) was extracted from the wiggler using the 'inclined-view method' (Cooper *et al.*, 1986), with the sample situated 2 mm above the orbital plane at 70 m from the source, giving an azimuthal angle of $\sim$30 μrad. Vertical slits in front of the sample extracted radiation in the range 0.5–3.5 mm (7–50 μrad) above the orbital plane to maximize the figure of merit $P_c I^{1/2}$, where I is the scattered intensity, for the radiation hitting the sample. This figure of merit gives the signal-to-noise ratio of the scattered beam, *i.e.* the ratio of the magnetic signal, which is proportional to $P_c I$, and the 'statistical noise' coming from the dominant charge scattering, which is proportional to $I^{1/2}$.

The X-rays were monochromated using the 331 reflection of an Si 220 bent crystal in Laue geometry. The asymmetry angle for the 331 reflection was 13.26°, the thickness of the crystal was 1.5 mm and the resulting bandwidth was calculated to be $\Delta E/E \simeq 5 \times 10^{-4}$, which was verified by measuring the elastic line from a Pb scatterer. This value ensured that the overall resolution of the experiment was always dominated by the solid-state detector for which $\Delta E/E \geq 10^{-3}$. The Bragg angle of the monochromator was tuned to give incident energies of 84.4, 167.2 and 256.0 keV corresponding approximately to $(1/6)mc^2$, $(1/3)mc^2$ and $(1/2)mc^2$. The beam size at the sample was limited by slits and was approximately 2×3 mm. The flux at the sample position at 100 mA of beam current for each incident energy is given in Table 1.

The ferromagnetic sample of Fe used in this investigation is a single-crystal disc containing 3% silicon by weight to stabilize the b.c.c. structure. The disc is of diameter 25 mm and thickness $\sim$0.25 mm with the [110] zone axis normal to the disc. The single-crystal slice was clipped between the pole pieces of an electromagnet and the [111] crystallographic direction was aligned with **H** and **K**. The field generated by the electromagnet was sufficient to saturate the magnetically soft Fe sample. The geometrical arrangement is shown in Fig. 1; a scattering angle of 150.0° was the maximum that could be achieved without the beam hitting the pole pieces. This scattering angle gave Compton peak energies of 64.5, 103.7 and 132.0 keV, respectively, for the three incident energies. High angles are desirable to

Table 2
Contributions to the resolution at the three different energies used.

ΔE_{det} is the energy resolution of the solid-state detector; ΔE_{geo} is the geometrical broadening due to the angular acceptance of the detector; ΔE_{div} is the contribution from the divergence of the source; and ΔE_{mono} is the contribution to the band pass due to the range of Bragg angles caused by the varying curvature of the monochromator from front to back surface. The overall resolution is also given in energy (keV) and electron momentum [a.u. – see equation (7)]

E_i (keV)	E_f (keV)	ΔE_{det} (keV)	ΔE_{geo} (keV)	ΔE_{div} (keV)	ΔE_{mono} (keV)	Total resolution (keV)	Total resolution (a.u.)
84.4	64.5	0.376	0.066	0.002	0.020	0.380	0.51
167.2	103.7	0.465	0.166	0.008	0.090	0.485	0.42
256.0	132.0	0.505	0.273	0.017	0.210	0.555	0.39

minimize geometrical broadening effects in the line shape and to maximize the resolution of electron momentum at a given energy; a different magnet geometry, as recently designed by the authors, will permit a larger sample volume to be irradiated and a higher scattering angle to be chosen in future.

The magnetic field was flipped parallel and antiparallel to the scattering vector, and the spin-up and spin-down spectral data accumulated and saved separately. The counting time in each position was 10 s with a 0.5 s interval to ramp the field. The total data-collection times for each incident energy, along with the respective Compton intensities, are shown in Table 1, where the count rates into the detector are also given. These data highlight clearly the diminished flux at the highest energy (the critical energy of the wiggler is only 43 keV) which would only be partially offset by greater sample thickness that would, in any event, increase parasitic multiple scattering. Despite the limited count rate, sufficient beamtime was available for good statistical accuracy to be obtained. The stability of the beam, together with long half lives in excess of 24 h and the signal averaging technique, ensured that the errors in the data were purely statistical.

3.2. *The resolution function at high energies*

For magnetic Compton-scattering experiments performed at energies up to ~60 keV, the resolution of the experiment is dominated by the energy resolution of the germanium solid-state detector. Good detectors have a typical resolution of ΔE_{det} = 360 eV at 60 keV. In a Compton experiment at that energy, it is usually the detector response that dominates the momentum space resolution, leading to values for Δp_z = 0.6 a.u. [following equation (6)]. However, in going to higher energies, other contributions to the momentum space resolution become increasingly important. They are (*a*) the geometrical broadening caused by the finite size of the detector aperture ΔE_{geo}, (*b*) the broadening due to the divergence of the X-rays from the source Δ_{div}, and (*c*) the energy broadening ΔE_{mono} due to reflection of the incident beam off the front and back edges of the monochromator crystal. Table 2 shows the individual contributions from each of these effects for the three incident energies used in this investigation. They are independent and therefore add in quadrature to produce the overall instrumental resolution. If we consider only the detector resolution, there is an advantage in going to higher energies because the effective resolution of the Compton line shape improves, as explained earlier. In this study, the energy resolution of the Ge detector was determined using radioisotopes with gamma lines at energies close to the Compton peak energies, *i.e.* the 59.54 keV γ-emission line of a ^{241}Am radioisotope for the 84.4 keV measurement (Compton peak at 64.5 keV) and the 136.45 keV line from ^{57}Co for the 256.0 keV measurement (Compton peak at 132 keV). An extrapolation of the detector resolution was then used to determine the resolution for the intermediate energy measurement for which no suitable radioisotope was available. The deterioration of the resolution due to geometrical broadening depends on the range of scattering angles seen by the detector which, in turn, governs the range of Compton-scattered energies detected. In this experiment, the range of scattering angles was 150.0 ± 0.5°. As the incident energy increases, the range of Compton-scattered energies seen increases and the geometrical broadening starts to become an important effect. At the highest energy used in this investigation, ΔE_{geo} was approximately half ΔE_{ins} (see Table 2).

The synchrotron radiation coming from the source diverges naturally. This divergence means that the X-rays arrive at the surface of the crystal monochromator at varying angles and leave with a range of energies. This is always the case except when the source lies on the Rowland circle. Then the radius of curvature of the crystal compensates exactly for the divergence of the incoming beam so that the angle between the incoming beam and the crystal is always the same, and therefore there is no spread in the bandwidth of the incident energy arriving at the sample. In this study, the source was not sitting on the Rowland circle but was only 4 m (in 59 m) away, so the effect of the diverging beam on the crystal was very small, leading to incident band widths of $\Delta E_{div}/E_i \simeq 10^{-4}$; therefore this smearing effect was negligible. A more important effect in the monochromator is the polychromatic broadening which occurs in bent crystals simply because the angle between an incident ray and the crystal planes is not constant through the thickness of the crystal and the lattice spacing changes. The width of the energy band reflected

by the monochromator is approximately proportional to the thickness and the asymmetric cut of the crystal (Suortti, 1992). Numerical values calculated from the width of the rocking curve are given in Table 2.

Although the instrumental resolution dominates the resolution, contributions from geometrical broadening and polychromatic broadening in the monochromator are significant. The final resolution function is given by the convolution of each of these effects, and therefore depends also on the shape of each individual resolution function. The detector response function has a Gaussian form but the geometric and polychromatic contributions are closer to 'box' functions. Convoluting these three functions together does not significantly change the Gaussian shape because of the dominance of the detector response function. The momentum resolution is superior to that reported in earlier experiments by the Warwick group and at the two higher energies it represents a considerable improvement over what was previously possible. The overall energy and momentum resolutions are shown in Table 2.

4. Data analysis

The analysis of magnetic Compton profiles is simpler than for non-magnetic data because many of the systematic errors are eliminated when the difference between the 'up' and 'down' data is taken. Corrections must be applied for (*a*) the energy-dependent correction for absorption in the sample, (*b*) the decrease in efficiency of the Ge detector with increasing energy, (*c*) the correction for the energy dependence of the charge and magnetic scattering cross sections, and finally (*d*) conversion of the data from the energy to the momentum scale. In principle, a correction should be applied for multiple magnetic scattering (Sakai, 1987) but an estimate confirmed that the sample was sufficiently thin, especially for the higher energies, that no multiple-scattering correction was necessary. The other corrections were applied to the data sets for each field direction separately and then the difference was formed to yield $J_{\rm mag}(p_z)$. The magnetic effect, R, is given in Table 1 and defined by $(I^+ - I^-)/(I^+ + I^-)$, where I^+ and I^- are the intensities of scattered photons for the magnetization parallel and antiparallel to the scattering vector, respectively.

Unlike in previous magnetic Compton experiments (Lawson *et al.*, 1995; Zukowski *et al.*, 1993; Cooper *et al.*, 1993), there was no need to monitor the incident beam flux. The stability of the ESRF source and its long half life, coupled with the signal averaging technique, were adequate. Time series of data blocks were checked against the accumulated totals to verify that there were no 'bad' blocks before they were added in to the total. The corrected magnetic profiles are shown in Fig. 2. They have all been normalized to the same area and it is clear that they have identical line shapes, the most prominent feature being the central dip of more than 50%. The fact that the line shape recovered from these data is invariant with energy implies that the functional form of the cross section [see equation (4)] developed for low energies remains valid at least up to $(1/2)mc^2$. Furthermore, the magnetic effect approximately scales according to equation (4), as can be seen in Table 1.

The second important result from this study is the evident improvement in the experimental resolution. Fig. 3 shows the magnetic Compton profile measured at E_i = 167.2 keV along with the theoretical FLAPW calculation profile given by Kubo & Asano (1990), which has been convoluted with the appropriate resolution function having a FWHM of 0.42 a.u. The profiles are normalized to an area of $2.07\mu_B$ between −8.0 and +8.0 a.u., this being the value predicted in the band calculation. In the inset to the figure, the unpublished result of Tanaka (1990), quoted by Sakai (1996) for this crystal direction but at a resolution of 0.85 a.u., is shown together with the same calculation smeared to the experimental resolution; in that result the central 'dip' is much less pronounced and the 'shoulder' at ~2 a.u. is not discernible. Our result, at a resolution FWHM of 0.42 a.u., shows these finer features. (The profile measured at E_i = 256.0 keV has the slightly better resolution FWHM of 0.39 a.u., but due to the low count rate those data are statistically too poor to use because the finer features of the profile are masked by the statistical noise).

5. Discussion

The size of the magnetic effect increases as we move to higher energies, roughly as predicted by equation (4), derived in the low-energy approximation for the cross section. The rate of increase is less than the theoretical prediction but this may be because the degree of circular polarization of the incident beam is not well established. This could arise, for example, from the difficulty of knowing precisely how far above the orbital plane the beam

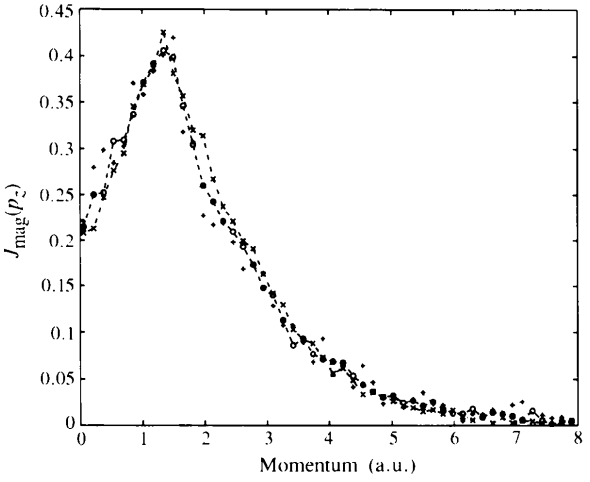

Figure 2
The magnetic Compton profile of Fe [111] measured with incident energies of 84.4 keV (dot-dashed line), 167.2 keV (○ points with dashed line) and 256.0 keV (+ points with dotted line). The area under each profile has been normalized to $2.07\mu_B$ between −8 and +8 a.u. The small decrease in profile widths with increasing energy reflects the improving resolution (see Table 2).

limiting slits are. An estimate of the probable uncertainty has been included in Table 1. It will be necessary to continue the measurements to higher energies in order to see if this deviation is real, due to the degree of circular polarization being different from that which the model predicts, or due to some other artefact. However, the fact that the magnetic profile line shape, $J_{mag}(p_z)$, and indeed the charge profile, $J(p_z)$, are invariant throughout this energy range indicates that the low-energy cross section still provides a viable model of the scattering process. Further improvements in resolution will be marginal because at backscattering the energy of the scattered beam does not increase in line with that of the incident beam and any small gain will certainly be offset by the deterioration in monochromator reflectivity, lower flux *etc.* These magnetic profiles were measured at the best resolution achieved to date without the use of a high-resolution spectrometer.

The low-resolution features of the directional magnetic Compton profiles of Fe are well known, particularly the 'volcano' structure with the central dip at $p_z = 0$. The Fe [111] directional profile has the largest central dip, but until the introduction of the FLAPW model calculations the theory always underestimated the size of this feature. Previously, the Fe [111] profile had not been measured at a resolution of better than 0.7 a.u., and the poorer resolution led to a smoothing out of the finer features of the profile. The depth of the observed central dip is a good way of comparing the magnetic Compton measurements made at increasing energies. In Fig. 2, where each of the profiles measured at the different energies were normalized to the same area but have different resolution, it can be seen that all three profiles have similar line shapes consisting of a central dip of ~60%. The slight narrowing of the profile with increasing energy reflects the improving resolution.

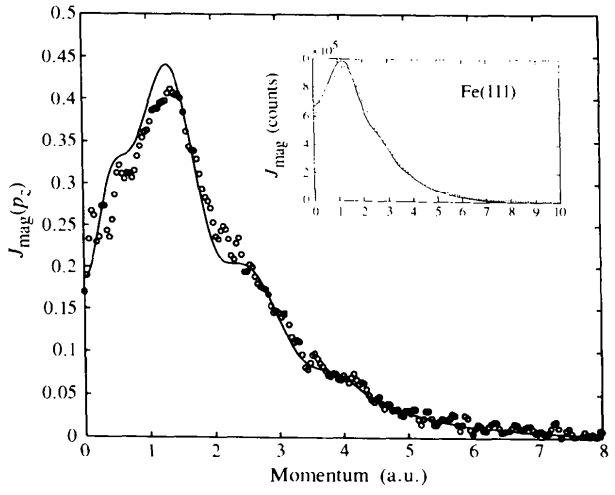

Figure 3
The magnetic Compton profile of Fe [111], measured with an incident energy of 167.2 keV, compared with the theoretical FLAPW profile of Kubo & Asano (1990) which is depicted by a solid line which has been convoluted with a Gaussian of 0.42 a.u. full width at half maximum. The experimental and theoretical results are normalized to the same area. The inset to the figure shows the unpublished result of Tanaka (1990) at the resolution of 0.85 a.u. quoted by Sakai (1996).

The measurement made with 0.42 a.u. momentum resolution at E_i = 167.2 keV has been normalized to the same area as the smeared FLAPW profile ($2.07\mu_B$ from –8 to +8 a.u.) with which it is compared; there is excellent agreement between these two profiles, the central dip corresponding to approximately 60% of the total profile. This dip is due to a negative contribution to the magnetization at $p_z < 1$ a.u. from the first band, which is due to negative polarization of the *s*-like electrons, and also a negative contribution from the second and third bands, which is mainly due to negative polarization of *p*-like electrons. The profiles fit well in the high-momentum tails, which confirms that the systematic corrections have been properly applied because energy considerations dictate that the high-energy tails cannot deviate significantly from the free-atom profile (Biggs, Mendelsohn & Mann, 1975). The shoulders at $p_z \simeq 0.5$ and 4 a.u. can be easily seen, although the feature predicted at 2.5 a.u. is not reproduced in these data. These features are not present in the magnetic Compton profiles of Fe [100] and Fe [110]. Looking at the individual electron bands (Kubo & Asano, 1990) it seems that the shoulder at $p_z \simeq 0.5$ a.u. comes from the fourth band contribution which has a maximum in this region, and that the main peak at $p_z \simeq 1.5$ a.u. comes from a combined contribution from the fourth, fifth and sixth bands. The shoulders at $p_z \simeq 2.5$ and 4 a.u. also come from the combined contributions of the fourth, fifth and sixth bands. In all previous experiments, these finer structures were not visible due to the low resolution but in this study they can be seen clearly.

The statistical accuracy achieved in this experiment was very good for the measurements made at 84.4 keV, adequate at 167.2 keV, and inadequate for the 256.0 keV measurement, which, despite its higher resolution, has lower information content than the result at the intermediate energy. There are a number of reasons for the low count rate at high energies in this experiment, all of which can be circumvented or alleviated in future studies. The main reason was the decrease in flux due from the wiggler at high multiples of the characteristic energy (the flux decreases by almost two orders of magnitude in going from 50 to 250 keV). Further high-energy studies at the ESRF will soon be improved by the use of a superconducting wavelength shifter (SCWS) which has a critical energy of 100 keV and provides higher flux than the asymmetric wiggler above 200 keV. At an incident energy of mc^2, with the sample sitting 2 mm above the orbital plane, the SCWS is two orders of magnitude brighter than the asymmetric wiggler for the same energy and provides almost as much flux as the latter does at $(1/2)mc^2$. A second point to consider is the efficiency of the Laue monochromator which decreases at higher energies, *e.g.* for the Si 331 reflection the peak reflectivity reduces from 62% at 84.4 keV to 22% at 167.2 keV and 10% at 256.0 keV. Improvements can be made by using a higher reflectivity cut and a thicker bent monochromator crystal.

With the use of the SCWS at the ESRF further studies are being made of the magnetic Compton cross section at energies near and beyond mc^2 with a view to investigating the breakdown of the low-energy model for inelastic scattering from bound electrons and optimizing the energy at which magnetic Compton experiments are performed in terms of the size of the magnetic effect and the resolution of the experiment.

We are grateful to the ESPRC (grant GR/H92401) for funding this investigation and to the authorities of the ESRF for allocating beamtime to this experiment and for providing a studentship (JMcC). We thank Veijo Honkimki for calculating the monochromator reflectivities, the beam polarization and for many helpful discussions and advice, and Y. Kubo and A. Asano for providing tabulated values of their FLAPW calculations. We acknowledge the valuable comments of the referees. This experiment forms part of a programme supported by the EU Human Capital and Mobility Initiative under contact ERB CHRXCT 930135.

References

Bell, F., Felsteiner, J. & Pitaevskii, L. P. (1996). *Phys. Rev. A*, **53**, R1213–1215.

Bhatt, G., Grotch, H., Kazes, E. & Owen, D. (1983). *Phys. Rev. A*, **28**, 2195–2200.

Biggs, F., Mendelsohn, L. B. & Mann, J. B. (1975). *At. Data Nucl. Data Tables*, **16**, 201–239.

Blume, M. (1985). *J. Appl. Phys.* **57**, 3615–3618.

Blume, M. & Gibbs, D. (1988). *Phys. Rev. B*, **37**, 1779–1789.

Bruckel, T., Bouchard, R., Kohler, T., Lippert, M., Neumann, H.-B., Poulsen, H. F., Rutt, U., Schmidt, T., Schneider, J. R. & von Zimmerman, M. (1995). *Rev. Sci. Instrum.* **66**, 1614.

Bruckel, T., Lippert, M., Kohler, T., Schneider, J. R. & Prandl, W. (1995). *J. Magn. Magn. Mater.* **140/144**, 1743–1744.

Carra, P., Fabrizio, M., Santoro, G. & Thole, B. T. (1996). *Phys Rev. B*, **53**, R5994–5997.

Cooper, M. J. (1985). *Rep. Prog. Phys.* **48**, 415–481.

Cooper, M. J., Laundy, D., Cardwell, D. A., Timms, D. N., Holt, R. S. & Clark, G. (1986). *Phys. Rev. B*, **34**, 5984–5987.

Cooper, M. J., Lawson, P. K., Dixon, M. A. G., Zukowski, E., Timms, D. N., Itoh, F., Sakurai, H., Kawata, H., Tanaka, Y. & Ito, M. (1996*a*). *Phys. Rev. B*, **54**, 4068–4074.

Cooper, M. J., Lawson, P. K., Dixon, M. A. G., Zukowski, E., Timms, D. N., Itoh, F., Sakurai, H., Kawata, H., Tanaka, Y. & Ito, M. (1996*b*). In preparation.

Cooper, M. J., Zukowski, E., Collins, S. P., Timms, D. N., Itoh, F. & Sakurai, Y. (1992). *J. Phys. Condens. Matter*, **4**, L399–404.

Cooper, M. J., Zukowski, E., Timms, D. N., Armstrong, R., Itoh, F., Tanaka, Y., Ito, M., Kawata, H. & Bateson, R. (1993). *Phys. Rev. Lett.* **71**, 1095–1098.

De Bergevin, F. & Brunel, M. (1972). *Phys. Lett.* A**39**, 141–142.

De Bergevin, F. & Brunel, M. (1981). *Acta Cryst.* A**37**, 314–324; 324–331.

ESRF Beamline Handbook (1994). Pp. 87–91. ESRF, Grenoble, France.

Grotch, H., Kazes, E., Bhatt, G. & Owen, D. A. (1983). *Phys. Rev. A*, **27**, 243–256.

Kubo, Y. & Asano, S. (1990). *Phys. Rev. B*, **42**, 4431–4446.

Lawson, P. K., McCarthy, J. E., Cooper, M. J., Zukowski, E., Timms, D. N., Itoh, F., Sakurai, H., Tanaka, Y., Kawata, H. & Ito, M. (1995). *J. Phys. Condens. Matter*, **7**, 389–400.

Lipps, F. W. & Tolhoek, H. A. (1954). *Physica*, **20**, 85–98; 395–405.

Lovesey, S. W. (1987). *J. Phys. C*, **20**, 5625–5639.

Lovesey, S. W. (1993). *Rep. Prog. Phys.* **56**, 257–326.

Mills, D. M. (1987). *Phys. Rev. B*, **36**, 6178–6181.

Platzman, P. M. & Tzoar, N. (1970). *Phys. Rev. B*, **2**, 3556–3559.

Platzman, P. M. & Tzoar, N. (1985). *J. Appl. Phys.* **57**, 3623–3625.

Ribberfors, R. (1975). *Phys. Rev. B*, **12**, 2067–2074.

Sakai, N. (1987). *J. Phys. Soc. Jpn*, **56**, 2477–2485.

Sakai, N. (1992). *Mater. Sci. Forum*, **105/110**, 431–438.

Sakai, N. (1994). *J. Phys. Soc. Jpn*, **63**, 4655–4656.

Sakai, N. (1996). *J. Appl. Cryst.* **29**, 81–89.

Sakai, N., Ito, M., Kawata, H., Iwazumi, T., Ando, M., Shiotani, N., Itoh, F., Sakurai, Y. & Nanao, S. (1991). *Nucl. Instrum. Methods Phys. Res. A*, **303**, 488–494.

Sakai, N. & Ôno, K. (1976). *Phys. Rev. Lett.* **37**, 351–353.

Sakai, N., Terashima, O. & Sekizawa, H. (1984). *Nucl. Instrum. Methods*, **221**, 419–426.

Sakurai, Y., Tanaka, Y., Ohata, T., Watanabe, Y., Nanao, S., Ushigami, Y., Iwazumi, T., Kawata, H. & Shiotani, N. (1994). *J. Phys. Condens. Matter*, **6**, 9469–9475.

Suortti, P. (1992). *Rev. Sci Instrum.* **63**, 942–945.

Tanaka, Y. (1990). Private communication cited in Sakai (1996).

Timms, D. N., Brahmia, A., Cooper, M. J., Collins, S. P., Hamouda, S., Laundy, D., Kilbourne, C. & Saint Lager, M.-C. (1990). *J. Phys. Condens. Matter*, **2**, 3427–3429.

Timms, D. N., Zukowski, E., Cooper, M. J., Laundy, D., Collins, S. P., Itoh, F., Sakurai, H., Iwazumi, T., Kawata, H., Ito, M., Sakai, N. & Tanaka, Y. (1993). *J. Phys. Soc. Jpn*, **62**, 1716–1722.

Zukowski, E., Collins, S. P., Cooper, M. J., Timms, D. N., Itoh, F., Sakurai, H., Kawata, H., Tanaka, Y. & Malinkowski, A. (1993). *J. Phys. Condens. Matter*, **5**, 4077–4090.

Zukowski, E., Cooper, M. J., Armstrong, R., Ito, M., Collins, S. P., Laundy, D. & Andrejczuk, A. (1992). *J. X-ray Sci. Tech.* **3**, 300–310.